scientific reports

Check for updates

OPEN

Optimization of alumina leaching from microcline using particle swarm optimization and response surface methodology

Ikechukwu A. Nnanwube[1]✉, Okechukwu D. Onukwuli[2], Monday Omotioma[3], Chinyere B. Ezekannagha[1], Christopher N. Igwilo[4], Chizoo Esonye[5], Valentine C. Anadebe[5] & Cyril S. Ume[5]

Alumina has found wide application in technological and engineering fields. However, due to the environmental effects of the traditional Bayer process of production, there is a need for a more eco-friendly and cost-effective procedure. The optimization of alumina extraction from microcline in nitric acid (HNO_3) solution is considered in this work. The optimization exercise was performed with the optimization tools of response surface methodology (RSM) and particle swarm optimization (PSO). The optimum conditions predicted by RSM include 82.11 °C reaction temperature, 3.53 M HNO_3 concentration, 0.023 g/mL solid/liquid (S/L) ratio, 356.14 rpm stirring speed, and 99.92 min reaction time. At these conditions, about 83.21% alumina leaching rate was predicted. PSO however predicted optimum conditions of 90°C, 4 M, 0.021 g/mL, 420 rpm, and 118 min, respectively, for the parameters above. Hence, the two techniques were viable tools for the optimization exercise.

Keywords Alumina, Microcline, Nitric acid, Optimization, Leaching

Aluminium is the most common metal in the earth's crust and the second most popular metal for making things. Due to its many unusual combinations of properties such as low density, corrosion resistance, electrical conductivity, ductility, and strength in alloys, aluminium and its compounds have found application in many industrial and commercial sectors such as food and drink packaging, aviation, automobile, building and construction, clothing, power cables, cooking utensils, to mention a few. On the other hand, alumina has been extensively deployed in progressive technological sectors, which include its application for the manufacture of microelectronics, good semiconductors, ceramics, biofuel and cell-fuel, insulators, high-strength materials, fireproof plastics, refractories, and high-grade polishes[1]. The metallic aluminium is not found in nature but occurs in the form of hydrated oxide or silicate (clay). The increasing demand for aluminium globally and the unavailability of bauxite in many countries increases the need to develop alternative technologies for the production of aluminium from low-grade ores[2].

Researchers in many countries have put in rigorous effort into alumina extraction from natural sources other than bauxite, particularly clays[3]. The use of clay as the natural resource for alumina recovery is preferred due to the merits of the process such as its environment friendliness, ready availability, and cost-effectiveness. This is in contrast to the Bayer process which is characterized by the generation of toxic residues and their attendant negative environmental consequences as well as the incurred cost of residue disposal. The choice of this process (clay process) would also help create job opportunities in communities where it is found as well as improve the gross domestic product (GDP) of Nigeria and attract foreign investment to Africa in line with African Union Agenda 2063, as well as promote responsible consumption and production, innovation, economic growth and industrial revolution, in line with the United Nations (UN) sustainable development goals[4].

Clays are hydrous aluminium silicates that usually contain small amounts of impurities such as calcium, magnesium, potassium, sodium, or iron. Many clay contain as much as 30–40% alumina[5]. One of the most common processes of clay formation is the chemical decomposition of feldspar. Among the various clay minerals,

[1]Chemical Engineering Department, Madonna University, Akpugo, Nigeria. [2]Chemical Engineering Department, Nnamdi Azikiwe University, Awka, Nigeria. [3]Department of Chemical Engineering, Enugu State University of Science and Technology, P.M.B. 01660, Enugu, Nigeria. [4]Department of Science Laboratory Technology, Federal College of Agriculture, Ishiagu, Nigeria. [5]Department of Chemical Engineering, Alex Ekwueme Federal University, Ndufu-Alike, Nigeria. ✉email: ik.nnanwube@gmail.com

microcline proves to be a feasible alternative for alumina production owing to its substantial aluminium content. Microcline ($KAlSi_3O_8$) is a key rock-forming mineral in many rocks, especially pegmatite, granite, syenite, and metamorphic gneisses. Microcline is usually found jointly with feldspar; as well as in syenite, granite, and pegmatites, critically characterizing acidic and neutral core igneous rocks[6].

Leaching involves materials extraction from a solid by dissolving them in a liquid, either through natural means, or through an industrial process. Leaching has various commercial uses in the chemical processing industry, including recovery of metal from its ore with the aid of acid, and sugar from sugar beets with the aid of hot water[2]. In extractive metallurgy, leaching is normally applied on account of its cost-effectiveness, environment-friendliness, low-energy requirement, and the capability of processing ores of low-grade. The three procedures generally applied for the recovery of alumina from clays include: (1) leaching using acids such as H_2SO_4, HNO_3 or HCl to remove alumina from clay after calcination, (2) sulphatization by sintering clay with ammonium sulphate and the subsequent removal of alumina by leaching using hot water, (3) alkali roasting by sintering of the clay with ammonium sulphate and the removal of alumina and silica by leaching using hot water[1].

Most acid-leaching procedures for alumina recovery have been conducted with the conventional one factor per time[1]. This procedure takes a long time and wastes a lot of reagents. To overcome this challenge, statistical and optimization techniques such as RSM which is made up of advanced statistical and mathematical procedures applied for process enhancement and optimization are adopted[7–9]. Using this method, optimum points are determined for given independent variables with the aid of a second-order polynomial prediction equation. Widely applied in the chemical industry, RSM helps in the improvement of manufacturing processes as well as optimizing chemical reactions to obtain products of high yield and purity at reduced cost[10,11].

On the other hand, PSO is a stochastic computation method[12]. Motivated by the social behaviour and intelligence of the insect swarm, PSO has continuously gained a rising reputation due to its ease and efficiency in performing hard optimization problems. It has been effectively applied in solving various optimization and engineering problems[13–16]. As obtainable in comparable evolutionary algorithms, PSO is an optimization technique that relies on a population often referred to as a swarm. Such a population comprises individual particles having specific positions and velocities produced at random during initialization. Particles look for a solution space and recall the overall best position it has established. Contrary to genetic algorithms, PSO does not need the process of encoding and special operators like crossover or mutation. The distinguishing feature of PSO is derived from particles' individual experiences, collaboration among particles as well as their aptitude to share knowledge[12].

In general, many investigators have tried to recover alumina from other alternative sources, such as kaolinitic clays using both alkaline and acid routes[17–19]. It was a common consensus that acids were more effective than bases in aluminium extraction[1]. Our previous publication on alumina recovery from microcline focused on the kinetics of the leaching process in nitric acid and hydrogen peroxide solution[6]. The process parameters were not optimized. Hence, in the present investigation, aluminium leaching from microcline through the nitric acid route was explored via optimization of process parameters. Process parameters that affect the leaching process were optimized and optimum points were determined using RSM and PSO.

Materials and methods

Materials

Sourcing and Preparation of samples

Microcline ore from Amagunze in south-eastern Nigeria was deployed for this work. The sample was ground, dried in the sun for two days, and calcined at 700 °C for 1 h to enhance its reactivity. The calcined microcline was further pulverized and sieved with < 75 µm ASTM standard test sieve and kept for further use. The solutions used in the experiment were prepared using analytical-grade nitric acid and deionized water.

Leaching experiments

Experiments were carried out according to the method described by Nnanwube and Onukwuli[20] and Nnanwube et al.[6]. The stoichiometry of the process is illustrated in Eq. (1).

$$Al_2O_{3(s)} + 6HNO_{3(aq)} \longrightarrow 2Al(NO_3)_{3(aq)} + 3H_2O_{(l)} \quad (1)$$

Design of experiment

The experimental design for alumina leaching from microcline via nitric acid leaching was executed with the central composite design of RSM. RSM is a set of mathematical and statistical tools which are helpful for the development of empirical models, enhancing and optimizing process parameters, as well as identifying the interaction between the factors that affect the response of interest, with a minimal number of experiments[21,22]. It utilizes numeric data from an associated experiment to establish a regression model as well as optimize a response which is affected by several of input factors.

The central composite design (CCD) of RSM is usually made up of a 2^n factorial runs with 2^n axial runs. The error in the experiment is estimated by centre runs (n_c). The variables are examined at two levels. However, as the variable number (n) rises, the number of runs necessary for a whole duplicate of the design increases speedily. Since the individual effect of second-order cannot be evaluated independently by 2^n factorial design, CCD was deployed to investigate the quadratic effects of the model for alumina recovery from Amagunze microcline[21]. In the statistical analysis, the response alongside the relevant parameters utilized in the process was modelled to optimize the process parameters for the response of interest. Statistical factors were evaluated using the analysis of variance (ANOVA)[23].

RSM involves three main steps which include the design of experiments, evaluation of coefficients in a developed mathematical model, and lastly, prediction of the response(s) and assessing the sufficiency of the model in the design space[24]. In this work, the five variables selected for the design include the reaction temperature (°C), S/L ratio (g/mL), nitric acid concentration (M), stirring speed (rpm), and reaction time (min). The range and levels of the factors deployed in the design are depicted in Table 1[25].

In carrying out the design, the variables in the experiments are presumed to be uninterrupted and measured by experiments with minimal errors. The design of the experiment was targeted at optimizing the response factor[21]. Hence, there is a need to find a proper estimate for the relation connecting the independent factors and the response. To minimize the error and the influence of unrestrained factors, the experimental run was arranged arbitrarily[26]. An empirical model generated using the response which relates it to the experimental variable is depicted by a second-degree polynomial equation presented as Eq. 2[27].

$$Y = \beta_0 + \sum_{i=1}^{n} \beta_i x_i + \sum_{i=1}^{n-1} \sum_{j=2}^{n} \beta_{ij} x_i x_j + \sum_{i=1}^{n} \beta_{ii} x_i^2 + \varepsilon \tag{2}$$

where Y denote the response predicted (alumina yield), $\beta_0, \beta_i, \beta_{ij}, \beta_{ii}$, n denotes the constant coefficient, linear coefficient, interaction coefficient, quadratic coefficient, and number of factors in the experiments, respectively; x_i and x_j denote the coded values of the variable parameters which affect the response, while ε denotes the models' random error[28,29]. The codes are estimated as a function of the range of interest of each factor as depicted in Table 1. Equation (3) represents the coding of the test variables in developing the regression model[30,31].

$$x_i = \frac{X_i - X_i^*}{\Delta X_i} \tag{3}$$

where x_i denotes the i^{th} independent factor of the dimensionless coded value; X_i denotes the uncoded value of the i^{th} independent factor; X_i^* denotes the uncoded value of the i^{th} independent variable at the centre point, while ΔX_i denote the step change[32].

The final equation for the five factors and the error of the model is depicted as Eq. (4).

$$\begin{aligned} Y = {} & \beta_o + \beta_1 A + \beta_2 B + \beta_3 C + \beta_4 D + \beta_5 E + \beta_{12} AB + \beta_{13} AC + \beta_{14} AD \\ & + \beta_{15} AE + \beta_{23} BC + \beta_{24} BD + \beta_{25} BE + \beta_{34} CD + \beta_{35} CE + \beta_{45} DE \\ & + \beta_{11} A^2 + \beta_{22} B^2 + \beta_{33} C^2 + \beta_{44} D^2 + \beta_{55} E^2 + \epsilon_i \end{aligned} \tag{4}$$

The standard particle swarm model

PSO was motivated by the swarming activities of animals and the social conduct of humans. A particle swarm consists of a populace of particles in which every particle is an object in motion[33]. It flies across the search space and is drawn to former locations it visited with a high fitness. Contrary to the entities in evolutionary estimation, particles do not reproduce nor be replaced by others[34,35]. In this model, the particles are prepared with a populace of arbitrary entrant solutions. The particles move iteratively across the d-dimension problem space to seek new solutions. Every particle possesses a position denoted by a position vector $\overrightarrow{p_i}$ (i denotes the particle index), as well as a velocity denoted by a velocity-vector $\overrightarrow{v_i}$. Every single particle recalls its own finest position so far in a vector $p_i^{\#}$ and its jth dimensional value is $p_j^{\#}$. The overall best position vector in the swarm until now is then deposited in a vector $\overrightarrow{p^*}$ and its jth dimensional value is p_j^*. In the course of the iteration time t, the updated velocity from the former velocity to the new velocity is estimated by Eq. (5). The new position is then estimated by summing the former position and the new velocity using Eq. (6)[36].

$$v_{ij}(t) = wv_{ij}(\text{t-1}) + \epsilon_1 r_1 (p_{ij}^{\#}(t-1) - p_{ij}(t-1)) + \epsilon_2 r_2 (p_j^{\#}(t-1) - p_{ij}(t-1)) \tag{5}$$

$$p_{ij}(t) = p_{ij}(\text{t-1}) + v_{ij}(t) \tag{6}$$

where r_1 and r_2 are arbitrary numbers, equally spread within the interval [0, 1] for the jth dimension of the ith particle. ϵ_1 and ϵ_2 are positive constants representing the coefficient of the self-recognition component and the coefficient of the social components, respectively[36]. w denotes the inertia factor which controls the extent the

Independent variable	Unit	Symbol	Coded variable levels				
			−α	−1	0	+1	+α
Leaching temperature	°C	X_1(A)	45	60	75	90	105
Acid concentration	M	X_2(B)	0.5	2	3.5	5.0	6.5
Solid/liquid ratio	g/ml	X_3(C)	0.01	0.02	0.03	0.04	0.05
Stirring rate	rpm	X_4(D)	75	230	385	540	695
Leaching time	min	X_5(E)	30	60	90	120	150

Table 1. Factors and level of various parameters of CCD design for alumina recovery from Amagunze microcline.

Component	Raw sample (%)	Calcined sample (%)	Component	Raw sample (%)	Calcined sample (%)
SiO_2	53.98	58.49	MgO	1.16	1.07
TiO_2	1.38	1.06	CaO	0.62	2.35
Al_2O_3	27.25	27.75	K_2O	3.61	3.63
Fe_2O_3	11.56	7.23	P_2O_5	0.14	0.07
Cr_2O_3	0.02	0.01	SO_3	0.19	0.24
ZnO	0.01	0.01	SrO	0.06	0.04
MnO	0.02	0.03	Cl	0.003	0.02

Table 2. XRF result of Raw and calcined Amagunze microcline[6].

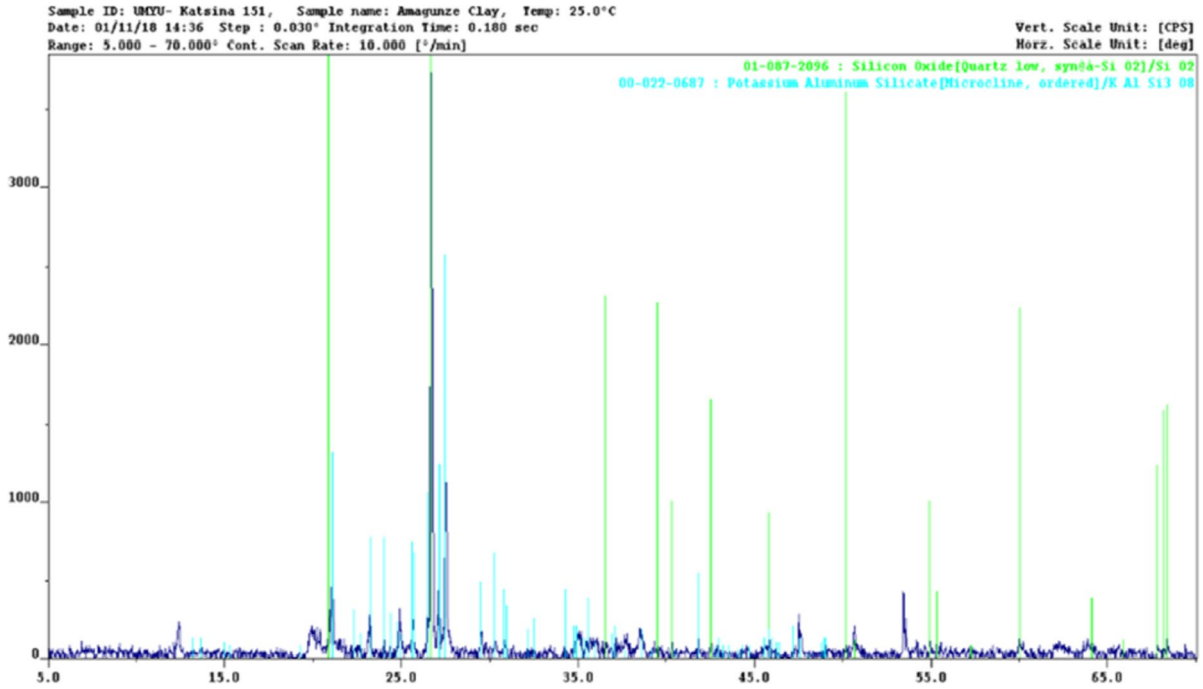

Fig. 1. XRD pattern of microcline.

particles tend to follow their present direction in comparison to the learnt positions[34,37]. It varies linearly from 1 to near zero for the period of the iterated processing. According to Eq. (5), a particle chooses where next to move, bearing in mind its peculiar experience, which depicts the reminiscence of its best former position and the experience of its most effective particle in the swarm[36].

Results and discussion

Characterization

XRF analysis

The XRF results of both the raw and calcined samples had previously been reported[6]. The result shows the main oxides in the clay as Al_2O_3, SiO_3 and Fe_2O_3, while the minor oxides are MgO, K_2O and TiO_2. Oxides found in traces include P_2O_5, SO_3, CaO, Cr_2O_3, ZnO, Mn_2O_3 and SrO, as shown in Table 2.

Mineralogical analysis

The XRD result of the clay confirms the presence of microcline ($KAlSi_3O_8$) with major peaks at 21.07, 26.44, 26.64, 27.11, and 27.45° 2θ, as earlier reported[6]. The XRD data is shown in Table 3 while the XRD pattern is shown in Fig. 1.

Statistical analysis

Statistical analysis of experimental data on alumina dissolution from microcline was performed with a rented version of Design Expert (DE) software 10.0.0. The CCD of RSM found in DE software was deployed to perform the regression analysis of the data generated from the experiment and plot the response surface and contour plots at the optimum conditions[21,38]. Several statistical indicators were used to fit the model and test the significance. F-test was used to examine the statistical importance of the models while the precision of the fitted polynomial model was established using the R^2 values[39]. The probability value (p-value) was deployed to assess

identifed, with their relative intensity (%)				
2θ	d-Value (Å)	Compound	intensity (%)	JCPDS file No.
20.86	4.25	Quartz (SiO_2)	21.62	01-087-2096
21.07	4.21	Microcline ($KAlSi_3O_8$)	51.00	00-022-0687
25.68	3.47	Microcline ($KAlSi_3O_8$)	26.00	00-022-0687
26.44	3.37	Microcline ($KAlSi_3O_8$)	41.00	00-022-0687
26.64	3.34	Quartz (SiO_2)	100.00	01-087-2096
27.11	3.29	Microcline ($KAlSi_3O_8$)	48.00	00-022-0687
27.45	3.25	Microcline ($KAlSi_3O_8$)	100.00	00-022-0687
36.55	2.46	Quartz (SiO_2)	6.01	01-087-2096
39.47	2.28	Quartz (SiO_2)	5.91	01-087-2096

Table 3. The X-ray diffraction data of Microcline showing the angle 2θ and d-values of the compounds identified, with their relative intensity (%). JCPDS File No. : Joint Committee on Power Diffraction Standards File Number.

the significant model terms at a 95% confidence interval. The experimental design, the coded, predicted and experimental values for this study, are depicted in Table 4[28].

For good quality model fitting, a test of significance for the regression model and separate model coefficients and lack-of-fit test is normally carried out. The sequential model sum of squares (Table 5) indicates that the quadratic vs. 2FI model is suggested with p-value of < 0.0001 and F-value of 76.71.

From the model summary statistics, it is shown that the R^2, adjusted R^2 and the predicted R^2 values of the quadratic model (0.9936, 0.9819, and 0.9198) gave a better fitting in comparison with the 2FI (0.7696, 0.5535 and − 2.0753) and the linear model (0.7493, 0.7010 and 0.6776) as depicted in Table 6[7]. The results above show that the quadratic model gave a good description of the correlation between the independent factors and the response (dependent variable).

For the model not to be over-fitted, the variance between the adjusted R^2 and predicted R^2 should not be more than 0.2. From the results obtained in this work, the variance between the adjusted and predicted R^2 for the quadratic model is 0.0117, indicating that the model is not over-fitted[40,41]. The adjusted R^2 measures the extent of difference around the mean described by the model, adjusted for the model number of terms; while the predicted R^2 measures the extent of difference in new data described by the model[42].

The quadratic model also gave a minimum standard deviation of 0.69, indicating a close connection between the predicted and experimental values of the responses[43].

The degree the model fits every point in the design is designated by the predicted residual error sum of squares (PRESS). It is estimated by first predicting where every single point should be from a model that comprises every other point except the one being considered.

To investigate if the process variables are statistically important or not, statistical analysis of variance (ANOVA) was performed. The ANOVA results are shown in Table 7.

The F-value for each variable indicates which variable had a considerable effect on the response which is the percentage of alumina leached[44,45]. The residual row shows the extent of disparity in the response that is yet to be explained while the Lack of Fit is the degree of variance between the model predictions and the observations[10,46,47].

The F-value of 85.06 from the model implies the model is significant. There is just a 0.01% probability that an F-value as large as this could occur because of noise. The change associated with a term and its residual variance is indicated by the F-value of that term. The F-value of the independent factors A, B, C, D, and E were obtained as 259.00, 260.27, 300.11, 240.19 and 223.28, respectively, signifying that the effect of all the independent variables on the response was significantly high. "Prob > F" values less than 0.050 implies that the model terms are important. The "Lack of Fit F-value" of 0.66 indicates that the Lack of Fit is not significant when compared to the pure error. There is a 68.91% chance that a "Lack of Fit F-value" this large could happen because of noise[48,49]. The lack of fit being insignificant is good since it indicates that the model fits. The significant and non-significant terms were determined from the ANOVA table (Table 5) in line with their p-values. From the ANOVA results, reaction temperature (A), nitric acid concentration (B), S/L ratio (C), stirring rate (D), reaction time (E), reaction temperature and stirring rate (AD), reaction temperature and reaction time (AE), reaction temperature squared (A^2), nitric acid concentration squared (B^2), S/L ratio squared (C^2), stirring rate squared (D^2), reaction time squared (E^2) are all significant[10]. The final polynomial predictive equation of the second order, after eliminating the insignificant terms is given in Eq. (7).

$$Y\,(\%) = 80.36 + 3.38 * A + 3.39 * B - 3.64 * C + 3.25 * D + 3.14 * E - 0.59 * AD - 0.68 * AE - 1.47 * A^2 - 2.25 * B^2 - 1.93 * C^2 - 2.27 * D^2 - 1.43 * E^2 \quad (7)$$

In terms of the actual factor values, the percentage yield of alumina is obtained and shown in Eq. (8).

Run	A: Leaching temp. (°C)		B: Acid conc. (M)		C: S/L ratio (g/mL)		D: Stirring rate(rpm)		E: Leaching time (min)		Yield (%)	
	Coded	Real	Coded	Real	Coded	Real	Coded	Real	Coded	Real	Exp.	Pred.
1	0	75	0	3.5	0	0.03	0	385	+2	150	81.8	80.90
2	0	75	0	3.5	0	0.03	0	385	−2	30	67.8	68.35
3	0	75	0	3.5	0	0.03	0	385	0	90	80.3	80.36
4	−1	60	+1	5	+1	0.04	−1	230	+1	120	68.1	67.95
5	+1	90	−1	2	+1	0.04	−1	230	+1	120	67.6	67.71
6	0	75	0	3.5	0	0.03	0	385	0	90	80.8	80.36
7	+1	90	−1	2	+1	0.04	+1	540	−1	60	68.2	68.11
8	0	75	+2	6.5	0	0.03	0	385	0	90	78.3	78.15
9	+1	90	+1	5	+1	0.04	−1	230	−1	60	69.5	69.23
10	−1	60	+1	5	+1	0.04	+1	540	−1	60	68.4	68.06
11	−2	45	0	3.5	0	0.03	0	385	0	90	67.4	67.72
12	0	75	0	3.5	0	0.03	0	385	0	90	80.3	80.36
13	−1	60	−1	2	+1	0.04	+1	540	+1	120	68.2	68.23
14	+2	105	0	3.5	0	0.03	0	385	0	90	81.9	81.23
15	−1	60	+1	5	−1	0.02	+1	540	+1	120	79.8	80.23
16	+1	90	−1	2	−1	0.02	−1	230	−1	60	69.2	69.36
17	−1	60	−1	2	−1	0.02	+1	540	−1	60	69.3	69.38
18	−1	60	−1	2	−1	0.02	−1	230	+1	120	69.1	69.37
19	+1	90	+1	5	+1	0.04	+1	540	+1	120	79.7	79.96
20	0	75	0	3.5	−2	0.01	0	385	0	90	80.9	79.90
21	0	75	0	3.5	0	0.03	0	385	0	90	81.8	80.36
22	+1	90	−1	2	−1	0.02	+1	540	+1	120	78.4	79.09
23	0	75	0	3.5	+2	0.05	0	385	0	90	64.7	65.35
24	0	75	0	3.5	0	0.03	−2	75	0	90	64.6	64.77
25	0	75	0	3.5	0	0.03	0	385	0	90	78.3	80.36
26	+1	90	+1	5	−1	0.02	−1	230	+1	120	80.1	80.61
27	+1	90	+1	5	−1	0.02	+1	540	−1	60	80.7	81.01
28	−1	60	+1	5	−1	0.02	−1	230	−1	60	68.2	68.10
29	0	75	0	3.5	0	0.03	+2	695	0	90	78.3	77.78
30	0	75	0	3.5	0	0.03	0	385	0	90	80.3	80.36
31	−1	60	−1	2	+1	0.04	−1	230	−1	60	50.2	49.70
32	0	75	−2	0.5	0	0.03	0	385	0	90	64.8	64.60

Table 4. Experimental design for alumina leaching from microcline using nitric acid.

Source	Sum of Squares	df	Mean Square	F-Value	p-value Prob > F	
Mean vs. Total	1.721E + 005	1	1.721E + 005			
Linear vs. Mean	1357.41	5	271.48	15.54	< 0.0001	
2FI vs. Linear	36.77	10	3.68	0.14	0.9983	
Quadratic vs. 2FI	405.84	5	81.17	76.71	< 0.0001	Suggested
Cubic vs. Quadratic	4.70	5	0.94	0.81	0.5814	Aliased

Table 5. Sequential model sum of squares.

Source	Std Dev.	R-Squared	Adjusted R-Squared	Predicted R-Squared	PRESS	
Linear	4.18	0.7493	0.7010	0.6776	584.15	
2FI	5.11	0.7696	0.5535	−2.0753	5571.46	
Quadratic	1.03	0.9936	0.9819	0.9198	145.29	Suggested
Cubic	1.08	0.9962	0.9802	0.7293	490.41	Aliased

Table 6. Model summary statistics.

Source	Sum of Squares	df	Mean Square	F-Value	*p*-value Prob > F
Model	1800.02	20	90.00	85.06	< 0.0001
A-Leaching temp.	274.05	1	274.05	259.00	< 0.0001
B-Acid conc.	275.40	1	275.40	260.27	< 0.0001
C-S/L ratio	317.55	1	317.55	300.11	< 0.0001
D-Stirring rate	254.15	1	254.15	240.19	< 0.0001
E-Leaching time	236.25	1	236.25	223.28	< 0.0001
AB	0.076	1	0.076	0.071	0.7942
AC	4.10	1	4.10	3.88	0.0747
AD	5.64	1	5.64	5.33	0.0414
AE	7.43	1	7.43	7.02	0.0226
BC	4.73	1	4.73	4.47	0.0581
BD	1.76	1	1.76	1.66	0.2242
BE	1.89	1	1.89	1.79	0.2083
CD	3.52	1	3.52	3.32	0.0956
CE	3.33	1	3.33	3.15	0.1037
DE	4.31	1	4.31	4.07	0.0687
A^2	63.43	1	63.43	59.94	< 0.0001
B^2	147.90	1	147.90	139.78	< 0.0001
C^2	109.60	1	109.60	103.58	< 0.0001
D^2	151.21	1	151.21	142.91	< 0.0001
E^2	60.23	1	60.23	56.92	< 0.0001
Residual	11.64	11	1.06		
Lack of Fit	5.14	6	0.86	0.66	0.6891
Pure Error	6.50	5	1.30		
Cor Total	1811.66	31			

Table 7. ANOVA for response surface quadratic model.

Std. Dev.	Mean	C.V. %	PRESS	Adeq. Precision
1.03	73.34	1.40	145.29	37.846

Table 8. Regression values.

$$\begin{aligned} Y\,(\%) = {} & -51.90 + 1.35 * \text{Leaching temp.} + 9.62 * \text{Acid conc.} + 162.72 * \text{S/L ratio} \\ & + 0.12 * \text{Stirring rate} + 0.53 * \text{Leaching time} - 2.55\text{E} - 004 * \text{Leaching temp.} * \text{Stirring rate} \\ & - 1.51\text{E} - 003 * \text{Leaching temp.} * \text{Leaching time} - 6.54\text{E} - 003 * \text{Leaching temp.}^2 \\ & - 1.00 * \text{Acid conc.}^2 - 19329.55 * \text{S/L ratio}^2 - 9.45\text{E} - 005 * \text{Stirring rate}^2 - 1.59\text{E} - \\ & 003 * \text{Leaching time}^2 \end{aligned} \quad (8)$$

The coefficient of variation is estimated by dividing the standard deviation by the mean and multiplying by 100[10,48]. Values less than 15% indicate a practically reproducible model. The coefficient of variation (CV) value of 1.40% obtained from this study illustrates that the model is practically reproducible. The signal-to-noise ratio depicted as the adequate precision is 37.846 as presented in Table 8. Ratios greater than 4 indicate that a good connection of signal-to-noise ratio exists. The mean is the overall average of all the response data. A value of 73.34 was recorded from this study[7,30].

The experimental results were also analyzed to verify the connection between the experimental and predicted alumina recovery. Figure 2 shows an adequate relationship between the experimental and predicted alumina yield. The result indicates also that the chosen model was sufficient for carrying out the prediction and optimization exercise[50–52].

Effect of process parameters

The effect of the variables that influence the leaching of alumina from microcline in HNO_3 solution was studied by conducting batch experiments at the pre-determined conditions obtained according to the experimental design. Experimental design was performed using the CCD of RSM, facilitated by the DE software by Stat Ease Inc., Minneapolis, USA. The interactive effect of the process variables was represented with contour and surface plots made with the software, according to the experimental results[50,53–55]. From the ANOVA results depicted in Table 7, the squared and individual effects of the factors were all significant with p-values < 0.0001, with the S/L ratio, acid concentration and leaching temperature, having the most significant effects, as specified by their

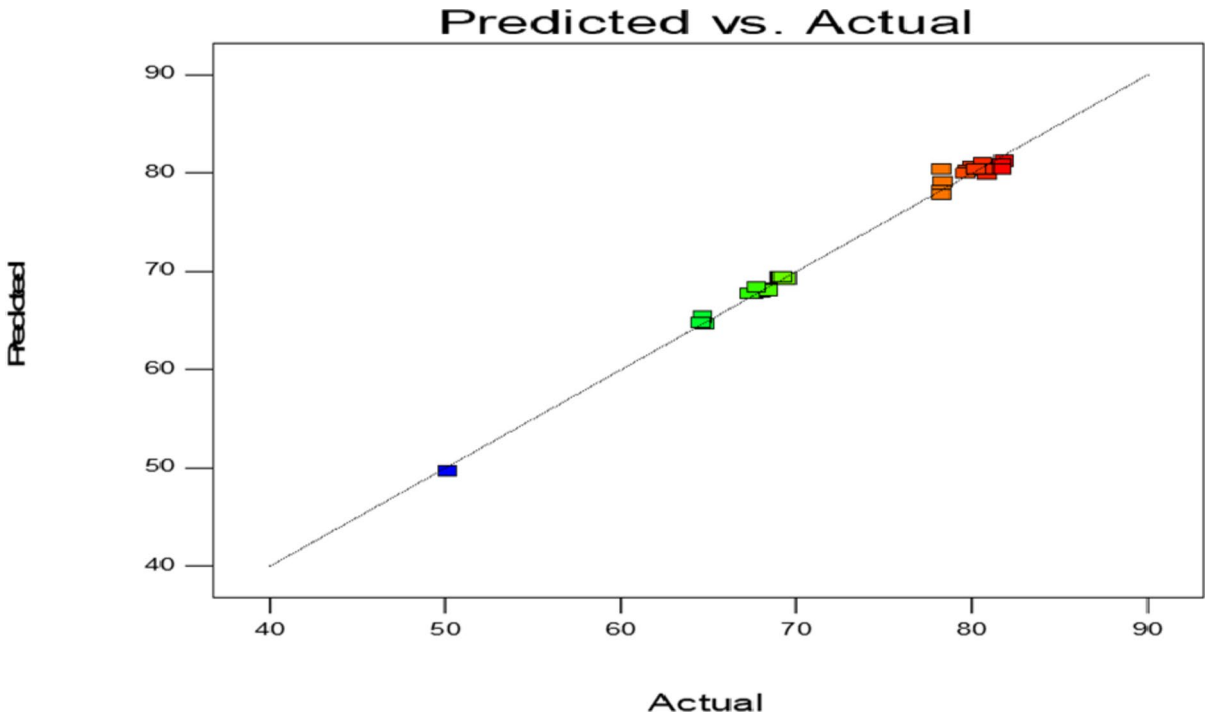

Fig. 2. Plot of the predicted values versus the actual experimental values.

F-values[10]. The interactive effects of stirring rate and leaching temperature (AD) as well as leaching temperature and leaching time (AE) were also found to be significant. Higher temperatures provide more energy for chemical reactions to occur faster, resulting in quicker dissolution of clay minerals. As temperature rises, the diffusion of ions through the clay particle's surface layer is facilitated, allowing for better access of the acid to the reactive sites. Increased temperature can increase mass transfer between the liquid phase (acid solution) and the solid clay particles, further improving the leaching process. While higher temperatures generally lead to better leaching efficiency, there is usually an optimum temperature range beyond which other factors like excessive energy consumption or potential side reactions might become significant. As acid concentration rises, more hydrogen ions are available to react with the clay minerals, breaking down the chemical bonds and releasing elements like aluminium and silica into the solution. Excessively high acid concentrations can result in significant damage to the clay's crystalline structure, potentially hindering further leaching by creating a less accessible surface area. For efficient clay leaching, finding the optimal acid concentration is crucial to maximizing the extraction of desired elements while minimizing unnecessary damage to the clay structure. When the solid/liquid ratio is high, fewer acid molecules are available to interact with each clay particle, limiting the reaction sites and slowing down the dissolution process. As more clay particles are present, diffusion of the dissolved ions away from the clay surface becomes more difficult, creating a concentration gradient that hinders further leaching. A lower solid/liquid ratio is generally preferred for efficient acid leaching of clays to maximize the contact between acid and clay particles. However, an optimum solid/liquid ratio is preferred for more efficient leaching. As stirring speed increases, the boundary layer surrounding clay particles thins, facilitating faster diffusion of the acid solution to the clay surface, thereby accelerating the leaching process. Better contact between the acid and clay particles due to increased stirring leads to a higher reaction rate, resulting in more minerals being dissolved within a given time frame. For more efficient leaching, optimum stirring speed should be used. As leaching time increases, more targeted elements are dissolved and removed from the clay structure, resulting in higher extraction efficiency. The initial phase of leaching often shows a rapid increase in extraction as the acid readily attacks the clay surface, with the rate gradually slowing down as the reaction progresses. Eventually, an equilibrium is reached where the rate of further extraction becomes negligible as most accessible minerals are already dissolved, indicating an optimal leaching time[56].

The contour and response surface plots are represented in Fig. 3 (a-d). Figure 3 (a and b) depict the joint effect of temperature and stirring speed on alumina leaching from microcline[10]. The results reveal that the highest alumina yield was achieved within a reaction temperature range of (72-78°C) and a stirring rate range of (354–416) rpm. Other variables were kept constant at a nitric acid concentration of 3.5 M, S/L ratio of 0.03 g/mL, and leaching time of 90 min. The percentage of alumina leached increased as the stirring rate was increased and attained a maximum at a stirring rate of 385 rpm. This shows that the stirring rate had a mild influence on the leaching rate of alumina[57]. On the other hand, the percentage alumina recovery rate increased with an increase in temperature up to a temperature of 75 °. This is ascribed to the destruction of the clay's structure at a higher temperature. The plot displaying the collaborative effect of temperature and time is depicted in Fig. 3 (c and d). The plot reveals that maximum alumina recovery was achieved within a temperature range of (78-84°C)

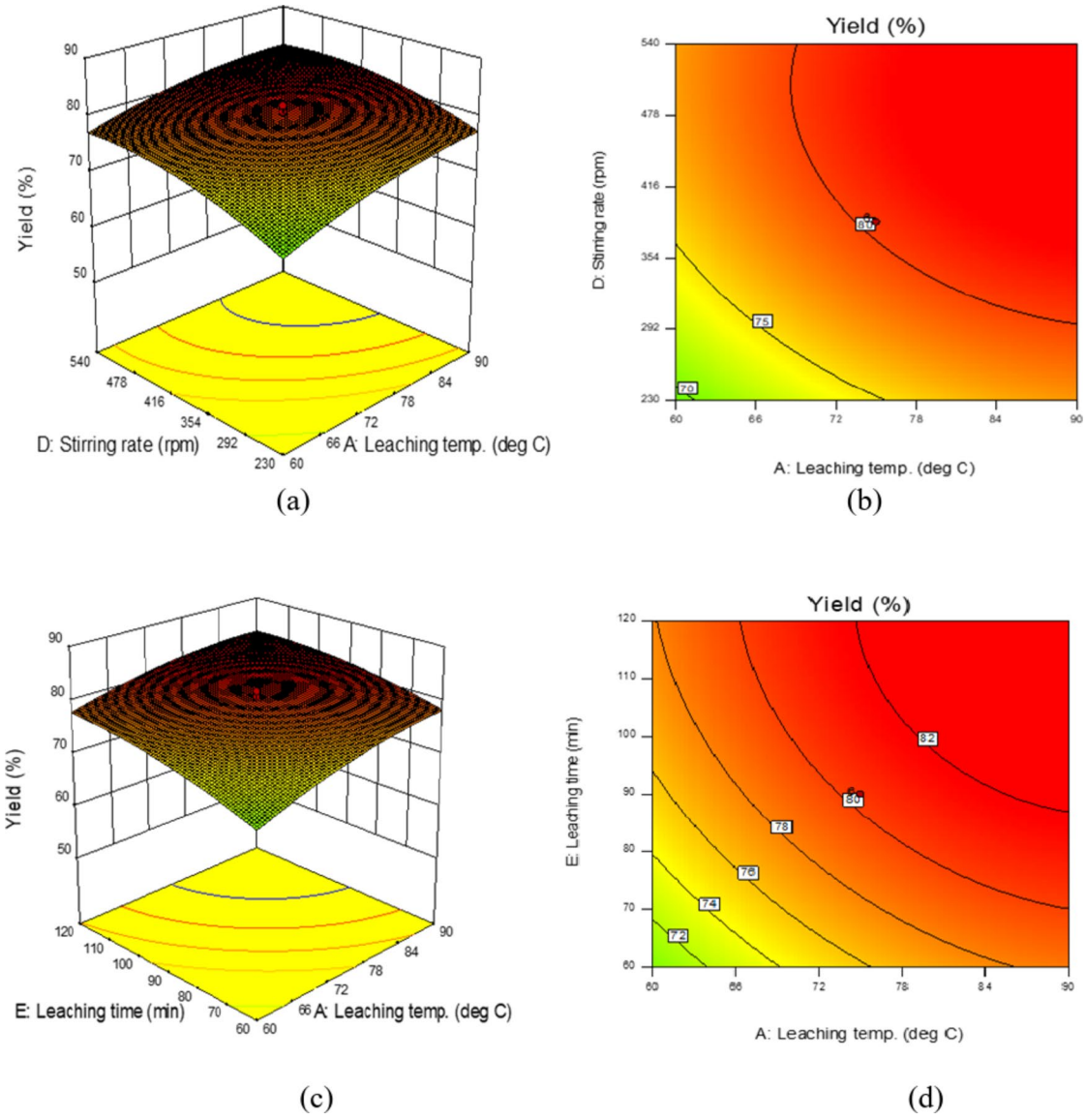

Fig. 3. 3D response surface (**a**, **c**) and contour (**b**, **d**) plots on the effects of process variables on alumina yield.

and a reaction time value of (90–100 min) while other factors were held constant at a HNO_3 concentration of 3.5 M, S/L ratio of 0.03 g/mL and stirring speed of 385 rpm. The amount of alumina recovered increased with an increase in leaching temperature up to a leaching temperature of 75°C and then decreased. The decrease in alumina recovery upon attainment of a leaching temperature of 75°C can be ascribed to the obliteration of the clay's structure at a higher temperature value[10]. The quantity of alumina leached was also found to increase as the leaching time was increased, up to 98 min and then decreased. The decrease in alumina recovery after 98 min may be due to the attainment of steady-state at a leaching time of 98 min.

Optimization using RSM and PSO

The optimization exercise was performed with the optimization apparatuses of the CCD of RSM in the design expert software and the particle swarm optimization in Matlab. In performing the RSM optimization exercise, the optimum points were selected based on cost implications which were aimed at reducing the cost of reagents, energy, and leaching time. Based on the above-named conditions, RSM predicted optimum conditions of 82.11°C reaction temperature, 3.53 M nitric acid concentration, 0.023 g/mL S/L ratio, 356.14 rpm stirring speed, and 99.92 min reaction time, at which about 83.21% alumina leaching rate was recorded[10]. The result obtained above was authenticated by performing three separate experiments at which an average alumina leaching rate of about 82.12% was recorded. PSO optimization was performed using a PSO algorithm developed in Matlab. Equation 8 was used to develop the objective function which was carried out in a Matlab file. The five factors used for RSM optimization were selected as assessment variables for particle swarm optimization. Other factors necessary for the simulation work were properly set in the PSO algorithm[10]. The initial weight damping ratio, the weight, and the swarm size were set to be 0.99, 1.0, and 30, respectively. The personal learning coefficient was set

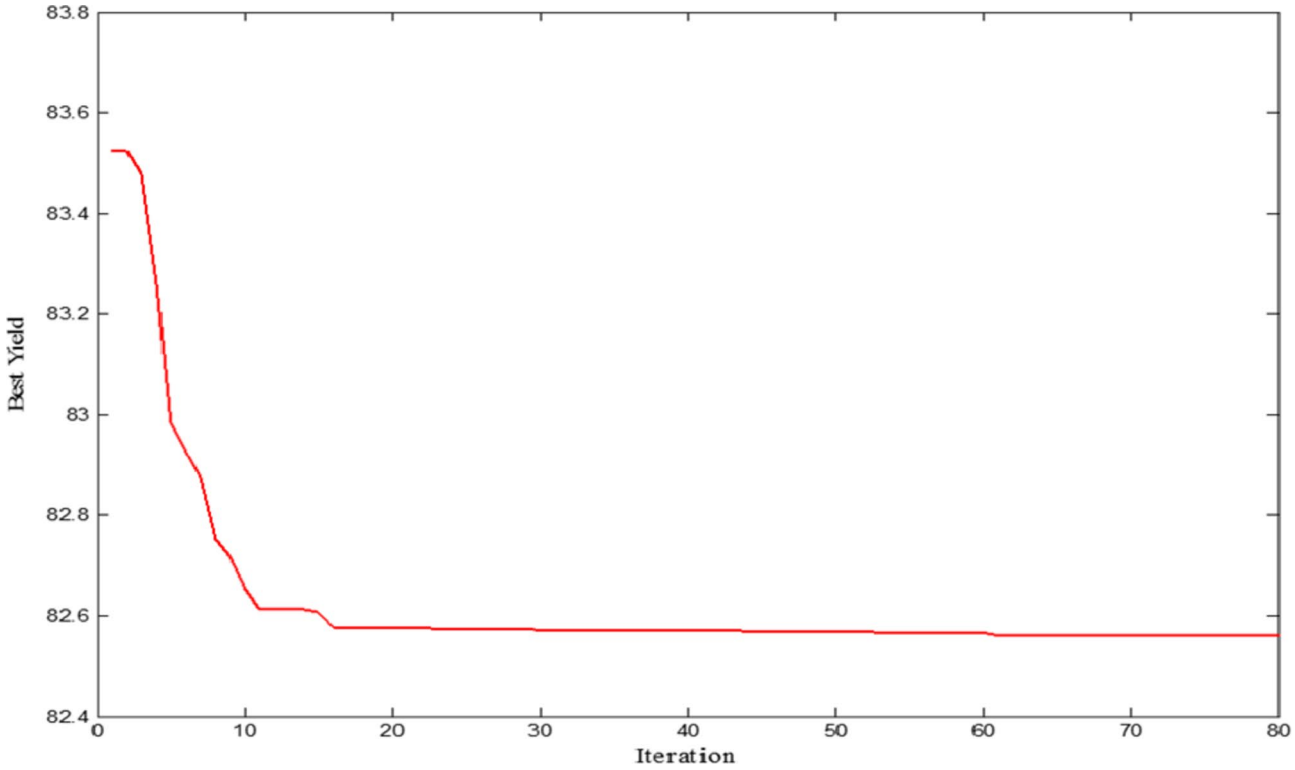

Fig. 4. PSO plot of alumina yield versus the number of iterations.

to be 1.2 while the global learning coefficient was set to be 2.0[58]. At the conditions stated above, PSO predicted optimum conditions of 90°C reaction temperature, 4 M nitric acid concentration, 0.021 g/mL S/L ratio, 420 rpm stirring speed, and 118 min reaction time, at which about 82.56% alumina leaching rate was predicted. The optimum conditions above were authenticated by performing three separate experiments which contributed an estimated average value of 81. 37%. The PSO plot of the percentage alumina yield versus the number of iterations is depicted in Fig. 4. In the RSM procedure, the optimum conditions were chosen from an array of options based on economic considerations. However, in PSO optimization, the minimum likely obtainable values of the experimental parameters (factors) are predicted, since PSO is a minimization tool. From the results attained in both optimization methods, a difference 7.89°C (8.77%), 0.47 M (11.75%), 0.002 g/mL (8.70%), 63.86 rpm (15.20%), and 18.08 min (15.32%) were recorded for the reaction temperature, HNO_3 concentration, S/L ratio, stirring speed, and reaction time, respectively. Hence, it can be inferred that the reaction time and stirring rate had a mild effect on the leaching process while the reaction temperature, HNO_3 concentration, and solid/liquid ratio had a more significant influence on the leaching process. When compared to the results obtained from the kinetic study, the two optimization techniques were found to be viable for alumina recovery from microcline.

Conclusions

The optimum conditions for alumina dissolution from Amagunze microcline were determined in this study. The mineral phases found in the clay as determined by XRD showed the presence of microcline as the major mineral present. XRF analysis result showed that the main oxides in the clay include Al_2O_3, SiO_3 and Fe_2O_3. Other oxides present in the clay sample include MgO, K_2O, CaO, Mn_2O_3, TiO_2, Cr_2O_3, ZnO, and SrO. Two optimization techniques which include the optimization tool found in the CCD of RSM of design expert software and the particle swarm optimization tool found in Matlab were used for the study. The optimum predicted conditions by RSM include reaction temperature of 82.11°C, HNO_3 concentration of 3.53 M, S/L ratio of 0.023 g/mL, stirring speed of 356.14 rpm and reaction time of 99.92 min, at which about 83.21% alumina leaching rate was predicted, while about 82.56% alumina leaching prediction was recorded by PSO at a reaction temperature of 90°C, nitric acid concentration of 4 M, S/L ratio of 0.021 g/mL, stirring speed of 420 rpm, and reaction time of 118 min, respectively. Hence, the two optimization methods proved to be feasible for alumina leaching.

Data availability

All data generated or analyzed during this study are included in this published article [and its supplementary information files].

Received: 21 November 2024; Accepted: 6 March 2025
Published online: 17 March 2025

References

1. Tantawy, M. A. & Alomari, A. A. Extraction of alumina from Nawan Kaolin by acid leaching. *Orient. J. Chem.* **35** (3), 1013–1021 (2019).
2. Nnanwube, I. A. Kinetics and optimization studies on the hydrometallurgical recovery of zinc, lead, and alumina from their parent matrices, PhD Thesis, Nnamdi Azikiwe University, (2019).
3. Al-Zahrani, A. A. & Abdul-Majid, M. H. Extraction of alumina from local clays by hydrochloric acid process. *JKAU: Eng. Sci.* **20** (2), 29–41 (2009).
4. Nnanwube, I. A., Keke, M. & Onukwuli, O. D. Kinetics of Owhe kaolinite leaching for alumina recovery in hydrochloric acid solution. *Sci. Afr.* **23**, e02045. https://doi.org/10.1016/j.sciaf.2023.e02045 (2024).
5. Nnanwube, I. A. & Onukwuli, O. D. Kinetics and mechanisms of nitric acid leaching of alumina from Amagunze clay. *J. Eng. Appl. Sci.* **13**, 63–82 (2018).
6. Nnanwube, I. A., Onukwuli, O. D. & Ekumankama, E. O. Assessment of Amagunze microcline for alumina recovery in nitric acid and hydrogen peroxide solutions and kinetic study. *Can. Metall. Q.* **62** (2), 330–344. https://doi.org/10.1080/00084433.2022.2099725 (2022a).
7. Nnanwube, I. A., Onukwuli, O. D. & Ajana, S. U. Modeling and optimization of Galena dissolution in hydrochloric acid: comparison of central composite design and artificial neural network. *J. Minerals Mater. Charact. Eng.* **6**, 294–315 (2018).
8. Nnanwube, I., Udeaja, J. & Onukwuli, O. Modeling and Optimization of Zinc Recovery From Enyigba Sphalerite in a Binary Solution of Acetic Acid and Hydrogen Peroxide, *Sigma Journal of Engineering and Natural Sciences*, 38(2) 589–601. (2020).
9. Nnanwube, I. A., Onukwuli, O. D., Obibuenyi, J. I., Okafor, V. N. & Ajemba, R. O. Optimization of colour pigments removal from palm oil using activated Ogbunike kaolinite. *Sigma J. Eng. Nat. Sci.* **38** (1), 253–263 (2020b).
10. Onukwuli, O. D. & Nnanwube, I. A. Optimization of zinc recovery from sphalerite using response surface methodology and particle swarm optimization: optimization of zinc recovery from sphalerite. *Periodica Polytech. Chem. Eng.* **66** (1), 20–29 (2022).
11. Nnanwube, I. A. & Onukwuli, O. D. Modeling and optimization of zinc recovery from Enyigba sphalerite in a binary solution of hydrochloric acid and hydrogen peroxide. *J. South. Afr. Inst. Min. Metall.* **120** (11), 609–616. https://doi.org/10.17159/2411-9717/1239/2020 (2020).
12. Borowska, B. Novel algorithms of particle swarm optimization with decision criteria. *J. Exp. Theor. Artif. Intell.* **30** (5), 615–635. https://doi.org/10.1080/0952813X.2018.1467491 (2018).
13. Jena, P. K., Thatoi, D. N. & Parhi, D. R. Dynamically self-adaptive fuzzy PSO technique for smart diagnosis of transverse crack. *Appl. Artif. Intell.* **29**, 211–232 (2015).
14. Liu, F. & Zhou, Z. An improved QPSO algorithm and its application in the high-dimensional complex problems. *Chemometr. Intell. Lab. Syst.* **132**, 82–90 (2014).
15. Garg, H. A hybrid PSO-GA algorithm for constrained optimization problems. *Appl. Math. Comput.* **274** (2016), 292–305 (2016).
16. Guedria, N. B. Improved accelerated PSO algorithm for mechanical engineering optimization problems. *Appl. Soft Comput.* **40**, 455–467 (2016).
17. Olaremu, A. G. Sequential leaching for the production of alumina from a Nigerian clay. *Int. J. Eng. Technol. Manage. Appl. Sci.* **3** (7), 103–109 (2015).
18. Dash, B., Das, B. R., Tripathy, B. C., Bhattacharya, I. N. & Das, S. C. Acid dissolution of alumina from waste aluminium Dross. *Hydrometallurgy* **92**, 48–53 (2008).
19. Pak, V. I., Kirov, S. S., Nalivaiko, A. Y., Ozherelkov, D. Y. & Gromov, A. A. Obtaining alumina from Kaolin clay via aluminium chloride. *MDPI: Mater.* **3938**, 1–12 (2019).
20. Nnanwube, I. A. & Onukwuli, O. D. Oxidative leaching of Akpugo kaolinite for alumina recovery and kinetic modeling. *J. Sustainable Metall.* **8** (4), 1727–1743. https://doi.org/10.1007/s40831-022-00603-y (2022).
21. Behera, S. K., Meena, H., Chakraborty, S. & Meikap, B. C. Application of response surface methodology (RSM) for optimization of leaching parameters for ash reduction from low-grade coal, *International Journal of Mining Science and Technology* 28 (4) (2018) 621- 629. (2018). https://doi.org/10.1016/j.ijmst.2018.04.014
22. Hameed, B. H., Lai, L. F. & Chin, L. H. Production of biodiesel from palm oil (Elaeisguineensis) using heterogeneous catalyst: an optimized process. *Fuel Process. Technol.* **90** (4), 606–610. https://doi.org/10.1016/j.fuproc.2008.12.014 (2009).
23. Singh, K. P., Singh, A. K., Singh, U. V. & Verma, P. Optimizing removal of ibuprofen from water by magnetic nanocomposite using Box-Behnken design. *Environ. Sci. Pollut. Res.* **19** (3), 724–738. https://doi.org/10.1007/s11356-011-0611-4 (2012).
24. Hafizi, A., Ahmadpour, A., Koolivand-Salooki, M., Heravi, M. M. & Bamoharran, F. F. Comparison of RSM and ANN for the investigation of linear alkylbenzene synthesis over $H_{14}[NaP_5W_{30}O_{110}]/SiO_2$catalyst. *J. Ind. Eng. Chem.* **19** (6), 1981–1989. https://doi.org/10.1016/j.jiec.2013.03.007 (2013).
25. Bhatia, S., Othman, Z. & Ahmad, A. L. Coagulation-flocculation process for POME treatment using Moringaoleifera seeds extract: optimization studies. *Chem. Eng. J.* **133** (1–3), 205–212. https://doi.org/10.1016/j.cej.2007.01.034 (2007).
26. Lebron, Y. A. R. et al. Statistical physics modeling and optimization of Norfloxacin adsorption onto grapheme oxide. *Colloids Surf., A*. **606**, 125534. https://doi.org/10.1016/j.colsurfa.2020.125534 (2020).
27. Nnanwube, I. A. & Onukwuli, O. D. Characterization and kinetics of alumina leaching from calcined Akpugo kaolinite for potential aluminum recovery. *S. Afr. J. Chem. Eng.* **43**, 24–37 (2023).
28. Obiora-Okafo, I. A. & Onukwuli, O. D. Optmization of coagulation-flocculation process for colour removal from Azo dye using natural polymers: response surface methodological approach. *Nigerian J. Technol.* **36** (2), 482–495. https://doi.org/10.4314/njt.v36i2.23 (2017).
29. Tran, T. N., Kim, D. & Ko, S. Encapsulation of biogenic manganese oxide and Pneudomonasputida MnB1 for removing 17 α-ethinylestradiol from aquatic environments. *J. Water Process. Eng.* **37** (2020), Article101423. https://doi.org/10.1016/j.jwpe.2020.101423 (2020).
30. Mahalik, K., Sahu, J. N., Patwardhan, A. V. & Meikap, B. C. Statistical modeling and optimization of hydrolysis of Urea to generate ammonia for flue gas conditioning. *J. Hazard. Mater.* **182** (1–3), 603–610. https://doi.org/10.1016/j.jhazm.2010.06.075 (2010).
31. Elibol, M. Optimization of medium composition for Actinorhodin production by streptomycescoelicolorA3 (2) with response surface methodology. *Process Biochem.* **39** (9), 1057–1062. https://doi.org/10.1016/50032-9592(03)00232-2 (2004).
32. Mallick, N., Gupta, S., Panda, B. & Sen, R. Process optimization for ploy (3-hydroxybutyrate- co-3-hydroxyvalerate) co-polymer production by Nostocmuscorum. *Biochem. Eng. J.* **37** (2), 125–130. https://doi.org/10.1016/j.bej.2007.04.002 (2007).
33. Kennedy, J. & Eberhart, R. C. Particle swarm optimization. In: Proceedings of the 1995 IEEE International Conference on Neural Networks. IEEE Press, Piscataway, NJ, 1942- 1948. (1995).
34. Paterlini, S. & Krink, T. Differential evolution and particle swarm optimization in partitional clustering. *Comput. Stat. Data Anal.* **50**, 1220–1247. https://doi.org/10.1016/j.csda.2004.12.004 (2006).
35. Dhahri, H., Alimi, A. M. & Karray, F. Designing bet a basis function neural network for optimization using particle swarm optimization. 2008 IEEE International Joint Conference on Neural Networks (IEEE World Congress on Computational Intelligence).
36. Liu, H., Abraham, A. & Zhang, W. A fuzzy adaptive turbulent particle swarm optimization. *Int. J. Innovative Comput. Appl.* **1** (1), 39–47 (2007).
37. Abderrahim, I. A., Loukil, L. & Hybrid PSO-TS approach for solving the quadratic three- dimensional assignment problem, 2017 First International Conference on Embedded and Distributed Systems (EDiS), 1–5. https://doi.org/10.1109/EDIS.2017.8284041

38. Luga, M. & Mironeasa, S. Simultaneous optimization of wheat heat moisture treatment and grape peels addition for pasta making. *Lebensmittel-Wissenschaftund-Technologie (LWT)*. **150** (2), 112011. https://doi.org/10.1016/j.lwt.2021.112011 (2021).
39. Singh, A. K. & Singh, K. P. Response surface optimization of nitrite removal from aqueous solution by Fe_3O_4 stabilized zero-valent iron nanoparticles using a three-factor, three-level Box-Behnken design. *Res. Chem. Intermed.* **42**, 2247–2265. https://doi.org/10.1007/s11164-015-2147-6 (2016).
40. Singh, H. K. G. et al. Refining of crude rubber seed oil as a feedstock for biofuel production. *J. Environ. Manage.* **203** (3), 1011–1016. https://doi.org/10.1016/j.jenvman.2017.04.021 (2017).
41. Li, X., Yang, Z., He, X. & Liu, Y. Optimization analysis and mechanism exploration on the removal of cadmium from contaminated soil by electrokinetic remediation. *Sep. Purif. Technol.* **250**, 117180. https://doi.org/10.1016/j.seppur.2020.117180 (2020).
42. He, Y., Perkins, D. & Huang, B. S-Box: A scalability analysis framework for ad hoc routing protocols. *Proceedings-International Symp. Computers Commun.* https://doi.org/10.1109/ISCC.2008.4625725 (2008).
43. Maleki, H., Duraes, L. & Portugal, A. Development of mechanically strong ambient pressure dried silica aerogels with optimized properties. *J. Phys. Chem. C.* **119** (14), 7689–7703. https://doi.org/10.1021/jp5116004 (2015).
44. Upadhyay, V., Jain, P. K. & Mehta, N. K. Modelling and experimental study of chip serration frequency in dry turning of Ti-6Al-4V alloy. *Int. J. Mach. Mater.* **12** (4), 358–371 (2012).
45. Kucuk, O. & Kocakerim, M. M. Optimization of dissolution of ulexite in water saturated with sulphur dioxide. *Chem. Eng. Process.* **44** (9), 1005–1011. https://doi.org/10.1016/j.cep.2004.11.006 (2005).
46. Inyang, V. & Lokhat, D. Reactive extraction of malic acid using trioctylamine in 1-decanol: equilibrium studies by response surface methodology using box Behnken optimization technique. *Sci. Rep.* **10**, 2400. https://doi.org/10.1038/s41598-020-59273-z (2020).
47. Singh, B. & Nanda, B. K. Slip damping mechanism in welded structures using response surface methodology. *Exp. Mech.* **52**, 771–791. https://doi.org/10.1007/s11340-011-9563-3 (2012).
48. Balbasi, M. Application of full factorial design method to silicalite synthesis. *Mater. Res. Bull.* **48** (8), 2908–2914. https://doi.org/10.1016/j.materresbull.2013.04.040 (2013).
49. Zhang, H. W. & Zhang, Y. D. Study on RSM procedure of Straightening process for aeronautical component based on finite element simulation. *Appl. Mech. Mater.* **42** (2010), 22–25. https://doi.org/10.4028/www.scientific.net/AMM.42.22 (2010).
50. Nnanwube, I. A., Keke, M. & Onukwuli, O. D. Assessment of Owhe kaolinite as potential aluminium source in hydrochloric acid and hydrogen peroxide solutions: kinetics modeling and optimization. *Clean. Chem. Eng.* **2**, 100022. https://doi.org/10.1016/j.clce.2022.100022 (2022b).
51. Elkelawy, M. et al. Maximization of biodiesel production from sunflower and soybeanoils and prediction of diesel engine performance and emission characteristics through response surface methodology. *Fuel* **266**, 117072. https://doi.org/10.1016/j.fuel.2020.117072 (2020).
52. Orugba, O. H., Onukwuli, O. D., Njoku, N. C., Ojebah, C. K. & Nnanwube, I. A. Process modelling of sulphuric acid leaching of Iron from Ozoro clay. *Eur. Sci. J.* **10** (30), 256–268 (2014).
53. Chakraborty, P., Dey, S., Parcha, V., Bhattacharya, S. S. & Ghosh, A. Design expert supported mathematical optimization and predictability study of buccoadhesive pharmaceutical wafers of Loratadine. *Biomed. Res. Int.* **2013**, 197398. https://doi.org/10.1155/2013/197398 (2013).
54. Nnanwube, I. A. et al. Equilibrium, kinetics and optimization studies on the bleaching of palm oil using activated Karaworo kaolinite. *J. Mater. Environ. Sci.* **11** (10), 1599–1615 (2020c).
55. Nnanwube, I., Udeaja, J., Onukwuli, O., Ugonabo, V. & Uwaleke, C. Modeling and optimization of zinc recovery from sphalerite using response surface methodology. *Maejo Int. J. Sci. Technol.* **14** (03), 283–292 (2020d).
56. Nnanwube, I. A., Keke, M. & Onukwuli, O. D. Assessment of calcined Owhe kaolinite for potential alumina recovery via nitric acid route, Results in Chemistry, 7(2024), Article no. 101262. (2024). https://doi.org/10.1016/j.rechem.2023.101262
57. Kansal, S. K., Singh, M. & Sud, D. Optimization of photocatalytic process parameters for the degradation of 2, 4, 6- Trichlorophenol in aqueous solutions. *Chem. Eng. Commun.* **194** (6), 787–802. https://doi.org/10.1080/00986440701193803 (2007).
58. Wang, C-C., Lin, Y-D., Wu, J-J., Lin, P-C. & Hwang, R. H. Toward optimal resource allocation of virtualized network functions for hierarchical datacenters, in IEEE Transactions on network and service management, 15(4) (2018) 1532–1544. (2018). https://doi.org/10.1109/TNSM.2018.2862422

Author contributions

I. A. N.: Conceptualization, Formal Analysis, Writing-Review & Editing, Software, Original Draft. O. D. O.: Supervision, Project Administration, Visualization. M. O.: Data Curation, Investigation, Methodology, Resources, Validation. C. B. E.: Resources, Validation. C. N. I.: Investigation, Methodology. C. E.: Formal Analysis, Methodology. V. C. A.: Software, Data Curation. C. S. U.: Methodology, Resources.

Funding

This research did not receive any specific grant from funding agencies in the public, commercial, or not-for-profit sectors.

Declarations

Competing interests

The authors declare no competing interests.

Additional information

Supplementary Information The online version contains supplementary material available at https://doi.org/10.1038/s41598-025-93326-5.

Correspondence and requests for materials should be addressed to I.A.N.

Reprints and permissions information is available at www.nature.com/reprints.

Publisher's note Springer Nature remains neutral with regard to jurisdictional claims in published maps and institutional affiliations.